EÖTVÖS LORÁND UNIVERSITY

FACULTY OF SCIENCE

INSTITUTE OF CHEMISTRY

LABORATORY OF INTERFACES AND NANOSTRUCTURES

DEPARTMENT OF PHYSICAL CHEMISTRY

Surface Modification of Fluorescent Carbon Quantum Dots

Supervisor:
Gyulai Gergő Dr.
Senior Lecturer

Author:
Bryan S. Chiguano Tapia
Materials Science MSc

Budapest, 2023

Contents

List of Figures

List of Tables

Statement of Intellectual Property

Name: Bryan Steven Chiguano Tapia

Neptun: GYSLIX

ELTE Faculty of Science: MSc Materials Science

Title of diploma work: Surface Modification of Fluorescent Carbon Quantum Dots.

As the author of the diploma work, I declare, with disciplinary responsibility that my thesis is my own intellectual product and the result of my own work. Furthermore, I declare that I have consistently applied the standard rules of references and citations.

I acknowledge that the following cases are considered plagiarism:

- using a literal quotation without quotation marks and adding citations;
- referencing content without citing the source;
- representing another person's published thoughts as my own thoughts.

Furthermore, I declare that the printed and electronic versions of the submitted diploma work are textually and contextually identical.

Budapest, 2023.

Bryan Steven Chiguano Tapia

Abstract

In this work, the optical, electrical, and particle size properties of physically and chemically modified fluorescent carbon quantum dots (CQD) were studied. CQDs were synthesized from citric acid and urea in DMF as solvent by a microwave-assisted synthesis process. EDA, ETA, and PEI were used for the modification of the CQDs. Purification of the raw CQDs and the subsequent modifications were performed through dialysis with a porous membrane. The particle's characterization was carried out by studying the hydrodynamic diameter, electrophoretic mobility, UV-Vis absorbance, fluorescence response, and ATR-IR spectroscopy.

Acknowledgements

I would like to express my sincere gratitude and appreciation to all those who have contributed to the completion of this thesis. First of all, I am deeply grateful to my supervisor, Dr. Gergő Gyulai, and MSc Dániel Fülöp for their guidance, expertise, and continuous support throughout the research process. Additionally, I am grateful for their assistance in data analysis, laboratory work, and technical support. Their valuable insights and encouragement have been essential in shaping this work.

I would like to express my gratitude to Eötvös Loránd University and Tempus Public Foundation for awarding me the Stipendium Hungaricum scholarship and providing me with the necessary resources and facilities to successfully complete this master's degree.

I would like to express my deepest gratitude to Dennis, Paulina, and Valeria for being my support and creating a sense of family. Their presence in my life has been an invaluable source of strength, offering me not only lessons and guidance but also countless memories throughout this journey.

Last but not least, my heartfelt appreciation goes to my parents Jorge and Rita, and my family and friends for their unwavering support, understanding, and encouragement during this academic journey.

Bryan Steven Chiguano Tapia

Budapest, June 2023

Chapter 1

Introduction

The new family of nanomaterials known as carbon quantum dots (CQDs) has attracted much attention in recent years. The carbon atoms that make up these nanoparticles, which are typically less than 10 nanometers in size, are clustered together in a crystalline or amorphous configuration. Due to quantum confinement effects, CQDs exhibit special optical and electronic characteristics that make them interesting candidates for use in various fields, such as optoelectronics, bioimaging, sensing, and energy storage [1–5].

One of the distinguishing features of CQDs is their tunable emission. The emission wavelength of CQDs, ranging from ultraviolet to near-infrared, can be fine-tuned by manipulating the size, surface functionalization, and synthesis techniques [6, 7]. In addition, CQDs exhibit high quantum yields, minimal toxicity, and high photostability, making them ideal for biological imaging and sensing applications [8]. They are useful for energy storage and optoelectronic devices because they also have good chemical stability, thermal conductivity, and electrical characteristics [2].

CQDs have demonstrated excellent potential in a wide range of applications. Their excellent optical properties make it possible to label and trace cells, tissues, and even individual biomolecules effectively in the field of bioimaging [8, 9]. CQDs can be used as fluorescent probes in detection applications to find various analytes, such as ions, heavy metals, and biological molecules [10]. In addition, due to their electrical characteristics, they can be used in LEDs, solar cells, and transistors [11–13]. Due to their large surface area and electrochemical stability, CQDs can also be used in energy storage systems such as super-

capacitors [14].

Carbon quantum dots have a bright future ahead of them. By investigating new synthesis techniques, surface engineering techniques, and device integration strategies, ongoing research aims to further improve the properties and functionalities of CQDs. To maximize the commercial potential of CQDs, scalable production methods need to be developed. In addition, scientists are actively studying how to combine CQDs with other materials and how to use them in cutting-edge sectors such as quantum computing and photovoltaics [15]. CQDs are expected to be widely used in many different technological fields as our understanding of them continues to expand.

The main aim of my research is to investigate the synthesis, characterization, and applications of carbon quantum dots with a specific focus on the surface modification of fluorescent CQD particles. By employing advanced synthesis techniques, such as microwave-assisted solvothermal methods, my goal is to synthesize luminescent and stable CQDs with controlled emission properties. Subsequently, a comprehensive characterization will be carried out using techniques such as UV-Vis, fluorescence, and ATR-IR spectroscopy, electrophoretic mobility by zeta potential analysis, and dynamic light scattering (DLS) to understand the structural, optical, and electronic properties of the synthesized particles. This research ultimately aims to contribute to the fundamental understanding and practical utilization of carbon quantum dots, paving the way for their broader applications in various fields.

Chapter 2

Theoretical Background

2.1 Carbon Quantum Dots

Carbon quantum dots (CQDs) are the newest addition to the carbon-based nanomaterials family. CQDs are nanoparticles with sizes ranging from 2 to 10 nanometers. They are fluorescent/photoluminescent particles. Their structure is composed of amorphous to nanocrystalline cores and shells made from polymer chains [5]. CQDs were first reported in 2004 when Xiaoyou Xu and coworkers found small carbon-containing, fluorescent fragments in the end-products of single-walled carbon nanotubes (SWCNTs) [16].

The term *carbon quantum dot* was introduced first by Sun et al. in 2006 [17]. CQDs are also found in the literature as carbon dots (CD), carbon nanodots (CND), graphene carbon dots (GCD), and polymer carbon dots (PCD). Although CQDs, CD, and CND are synonyms, their exact meanings may differ slightly depending on the synthesis method and characterization techniques used [1, 3–5, 18]. As a result, researchers must thoroughly characterize and describe their CQD samples to enable clear communication and accurate interpretation of results. In this work and hereafter, the nomenclature CQD or CQDs will refer to the studied particles.

2.1.1 CQDs Structure

The small size of CQD particles makes them ideal for utilization in several applications like medication administration, bioimaging, chemical sensing, catalysis, and optoelectronics.

CQDs have a high surface area-to-volume ratio due to their small size, allowing them to interact with neighboring molecules more effectively. This specificity and selectivity make them highly reactive toward various chemical species, such as metal ions, organic compounds, and biomolecules.

The properties of CQDs can be customized for specific applications by altering their surface using oxidation, reduction, and functionalization techniques. By introducing carboxyl groups, CQDs can undergo coordination with metal ions like Pb^{2+}, Hg^{2+}, and Sn^{2+}, forming stable complexes. This modification enables the creation of chemical detection devices capable of detecting contaminants even at lower concentrations [6, 7]. CQDs containing nitrogen atoms situated at the edge sites of aromatic domains can be effectively utilized in catalytic processes. These CQDs exhibit the ability to attract photogenerated electrons, leading to efficient charge separation and improved photocatalytic hydrogen generation from water [19]. Furthermore, nitrogen-containing CQDs derived from Kombucha fungus have been employed as electrode materials in supercapacitor structures, demonstrating excellent performance in charge and discharge processes [14]. The surface modification of CQDs can be accomplished through various straightforward and versatile methods, such as electrostatic assembly, covalent bonding, physical adsorption, and chemical adsorption.

Depending on the synthesis pathway (methodology, precursors, solvent, etc.), commonly, the CQDs consist of sp^2/sp^3 carbons and oxygen/nitrogen-based groups or polymeric aggregates. Several models have been proposed to describe the core of CQDs. These models describe diamond, graphite/graphite oxide, and amorphous carbon structures. This information has been verified by Fourier transform infrared (FTIR), high-resolution transmission electron microscopy (HRTEM), and X-ray diffraction (XRD). The molecular orbital theory can explain the electronic structure of CQDs. It has been studied that in most CQD particles, there are n $\rightarrow \pi^*$ and $\pi \rightarrow \pi^*$ transitions. CQDs' π states can be related to sp^2-hybridized aromatic carbons in the core. Functional groups containing lone electron pairs (carbonyls, amines, amides, and thiols) explain the n-states [2].

2.1.2 CQDs Optical Properties

Absorbance

CQDs absorb mostly, in the near-ultraviolet range, with lower absorption intensities in the visible and near-infrared regions. The surface groups can slightly modify the absorption

location, resulting in multicolored CQDs and the capacity to identify analytes colorimetrically [10]. For instance, self-passivated CQDs synthesized from a solvothermal procedure with PEG-200 have an absorption peak at 263 nm [20]; the fluorescent hydrophobic CDs [21] and carbogenic CQDs [22] produced from a microwave-assisted route show an absorbance peak at 242 and 285, respectively. The functionalization or modification of the CQDs' surface can shift the absorbance peak of the particles.

Photoluminiscence

The photoluminescence property of CQDs is one of their most fascinating characteristics. Previous studies have revealed a strong correlation between excitation and emission wavelengths and the intensity of CQDs. Several mechanisms have been proposed to explain the photoluminescence phenomenon of CQDs, including the quantum confinement effect, the surface state mechanism, the molecular state mechanism, and the crosslinking enhanced emission effect mechanism. The first mechanism, the quantum confinement effect, is determined by the carbon core of the CQDs. The second mechanism, the surface state mechanism, is influenced by the hybridization of the carbon backbone and the bonded chemical groups. Mechanisms 1 and 2 result in an increase in emission wavelength as the band gap narrows, which occurs gradually as the size of the sp^2 domains in the CQDs increases. The third effect, known as the molecular state mechanism, explains fluorescence as a direct consequence of an organic fluorophore on the surface of the CQDs. However, this mechanism is not applicable to particles produced at high temperatures, as it may lead to carbogenic aggregation and decomposition of the fluorophores. The fourth effect, the crosslinking enhanced emission effect mechanism, is specific to non-conjugated polymer carbon dots (PCDs). PCDs have shown enhanced fluorescence due to the crosslinking of the polymer chains, resulting in an intensified radiative transition [4, 5].

The remarkable photoluminescence exhibited by CQDs renders them highly valuable for optoelectronic applications, including light-emitting diodes (LEDs) and displays [13]. In a study conducted by Feng et al., CQDs with a high quantum yield were synthesized using a one-step hydrothermal method. These CQDs were then employed as a single white light converter for white light emitting diodes (WLEDs), with a UV-LED chip serving as the excitation light source. The resulting WLED exhibited exceptional performance that complied with international standards [23]. Furthermore, the integration of CQD particles into solar cell devices has opened up new possibilities in solar cell technology.

Tang et al. developed an all-weather solar cell by incorporating CQDs into their device. The fluorescence generated by the incident light in the 600 to 800 nm wavelength range was utilized for electricity generation. Under total darkness conditions, the device achieved a maximum photoelectric conversion efficiency of 15.1%, showcasing the potential for generating electricity throughout the day and inspiring the development of novel devices in the field [12].

2.1.3 Biological Properties

CQDs have received extensive research due to their distinctive biological characteristics and proposed biomedical uses. CQDs have several essential benefits, including low toxicity and high biocompatibility, which make them the perfect choice for biological applications. They may readily be functionalized with different biomolecules for targeted medication administration, bioimaging, and biosensing because they showed non-cytotoxic and biodegradable properties [8].

The application of CQDs in bioimaging has yielded outstanding outcomes. These CQDs have proven to be effective fluorescent probes for imaging various biological components such as cells, tissues, and organs, owing to their high quantum yields and photostability. In a study by Ada et al., biowaste-derived CQD particles synthesized through hydrothermal methods were utilized for imaging *E. coli* bacteria. By establishing H-bonds between the bacterial membranes and the CQDs, the fluorescence emitted by the CQDs enabled the identification of the bacteria [24]. Furthermore, CQDs have shown potential for targeted delivery of medications and biomolecules to specific cells or tissues. For instance, Zavareh et al. developed chitosan-based CQDs that facilitated the specialized targeted delivery of anti-cancer drugs for breast cancer treatment [25]. In addition to bioimaging and drug delivery, CQDs have displayed significant promise in biosensing applications. They can function as biosensors for detecting various substances, including DNA, proteins, glucose, and cancer cells. Glucose-based CQDs, in particular, have exhibited desirable characteristics as magnetic resonance imaging (MRI) contrast agents, emitting green fluorescence for the detection of cancer cells [9]. CQD-based biosensors offer several advantages over traditional biosensors, including heightened sensitivity, selectivity, and stability.

The antibacterial potential of CQDs is also investigated. They are strong candidates for novel antibacterial drugs due to their demonstrated antibacterial and antifungal activity.

CQDs are also used for tissue regeneration and wound healing because they encourage cell division and growth [26]. Antimicrobial mechanisms of CDs mainly include physical and mechanical destruction, reactive oxygen species (ROS-induced), oxidative stress, photocatalytic effect, and inhibition of bacterial metabolism. Travlou et al. have worked on developing sulfur- and nitrogen-doped CQD particles for bactericidal activity tests. Their work reports bacterial death linked to the electrostatic interactions between the protonated functional groups and the lipids of the bacteria's membrane [27].

2.2 Synthesis Methods of CQDs

In the last decade, several methods and techniques have been proposed and developed to synthesize CQDs. These can be summarized into two approaches: top-down and bottom-up approaches. Top-down methods involve breaking down a bulk material into smaller pieces through laser ablation or mechanical exfoliation. In this method, CQDs are produced from larger blocks of carbon materials by size and structure reduction, resulting in CQDs of smaller size and narrower size distribution. On the other hand, bottom-up methods involve building up material from individual atoms or molecules/precursors through chemical synthesis or self-assembly. Several techniques are used for CQDs synthesis like electrochemical carbonization, solvothermal/hydrothermal, and microwave irradiation. In this method, precursor molecules are used to build larger, structured CQDs, resulting in uniformly sized and well-defined CQDs [28, 29]. Both routes require an additional purification step that is usually carried out by dialysis or other techniques such as column chromatography or high-pressure liquid chromatography (HPLC) [18, 30, 31].

It is worth noting that the purification process is a crucial step in the production of CQDs. This process allows for the separation of unreacted molecules, solvent exchange, and fractionation of particles based on size or desired fluorescence properties. However, it is noteworthy that during the literature review, it was observed that a significant portion of the literature either lacks an in-depth discussion on this topic or only briefly mentions it as part of the synthesis process report. In many cases, the purification process is completely overlooked. Whichever approach, top-down or bottom-up, both have their advantages and limitations, the choice of method depends on the specific application and the desired properties of the final product.

2.2.1 Top-down Synthesis

Laser Ablation

The laser ablation technique utilizes a laser as an energy source to remove material from a solid sample in either a gas or liquid medium. Ablation refers to the process of eliminating material from the target surface through thermal evaporation. When aiming to create small particles, laser ablation in a gas medium is preferable. Conversely, laser ablation in a liquid medium is employed to disperse the nanoparticles within a liquid phase. Careful selection of the medium is necessary, as the particles generated by the laser tend to react readily with the surrounding molecules, potentially forming oxides and other undesired species. The purity of the nanoparticles obtained is highly dependent on the material of the target and the conditions of the medium, whether it is a gas or liquid [32].

Sun and his collaborators in addition to being credited with the name "quantum dots", synthesized bright and colorful photoluminescence CQDs by laser ablation [17]. Reyes et al. have reported that laser-ablated CQDs for light emission were synthesized from a carbon target material in a liquid medium. The obtained product showed a close-spherical amorphous shape within the size range of 5 to 20 nm and the particle abundance depended on the ablation parameters [33]. Liu et al. reported the synthesis of white-light-emitting materials via the formation of silicon and CD in silica nanoparticles [34]. Carbon nanoparticles could act as special structural scaffolds for the deposition of nanostructures of different transition metals, resulting in the production of useful nanocomposites that remain highly luminescent [35].

Pyrolysis

The pyrolysis technique involves the thermal decomposition of carbon-containing precursors in the absence of oxygen. Pyrolysis can be performed at high temperatures (usually above 500°C) and can produce CQDs with a high degree of crystallinity and a narrow size distribution. One of the main advantages of pyrolysis is the simplicity and versatility of the technique. It can be performed using a wide range of carbon sources, including organic compounds, biomass, and carbon-rich waste materials [36]. The size and optical properties of the CQDs produced by pyrolysis can be controlled by adjusting the reaction parameters such as the temperature, precursor concentration, and reaction time [37, 38]. For example, increasing the pyrolysis temperature can lead to the production of smaller

CDs (∼3 - 4) with higher fluorescence intensity [39]. The surface chemistry of the CQDs can also be modified by doping them with various elements such as nitrogen or phosphorus [36], or by functionalizing their surface with various organic or inorganic molecules. Functionalized CQD particles with poly l- lysine have been developed through one-pot pyrolysis method. The functionalized CQDs exhibited excellent antibacterial activity, bioimaging of bacterial cells through fluorescence microscopy, and antiangiogenesis [40].

2.2.2 Bottom-up Synthesis

Bottom-up synthesis involves a series of chemical processes that transform carbon-rich precursors into nanoparticles with specific properties. This method allows obtaining CQDs from a wide range of precursors. In general, the chemical processes that can occur during the synthesis of CQDs can be summarized as dehydration, condensation, polymerization, carbonization, surface functionalization, and purification [18]. Let's take as an example the citric acid/urea precursor mixture. Both precursors have been frequently used as carbon and nitrogen sources, respectively, for the production of CQDs [41–43].

The reaction mechanisms that can occur in the synthesis of CQDs from urea and citric acid can be different depending on the synthesis method, concentration of the reagents, and temperature, among other parameters. Let's take as an example the mechanism proposed by Kasprzyk et al. [44] and Strauss et al. [45] by using a hydrothermal process. They mention that at room temperature the mixture of the two reagents forms an eutectic mixture thanks to the interaction of hydrogen bonds. After applying heat to the mixture urea dissociates into isocyanic acid and ammonia. Then ammonia condenses with citric acid to form citrazinic acid, which reacts immediately with isocyanic acid to form HPPT (4-hydroxy-1H-pyrrolo[3,4-c]pyridine-1,3,6(2H,5H)- trione), a component related to the fluorescence phenomena in the core of CQDs. They also report that an excess of urea leads to the condensation of other types of products. They supported the obtained information through electron spray ionization mass spectrometry (ESI-MS), 2D- correlation nuclear magnetic resonance (2D-NMR), FTIR, X-ray photoelectron spectroscopy (XPS), X-ray diffraction XRD, and thermogravimetric analysis (TGA).

In the present investigation, the citric acid/urea pair was used as precursors and the synthesis was carried out by combining two techniques: solvothermal synthesis and microwave-assisted reaction. Some of the most commonly used techniques for the syn-

thesis of CQDs by the bottom-up approach are described below.

Electrochemical Carbonization

Electrochemical carbonization is generally considered a bottom-up method for the production of CQDs. This is because the CQDs are formed from the bottom-up through the electrochemical reactions of a precursor carbon source, such as graphite or carbon nanotubes, to generate small carbon clusters that can then be further processed to form CQDs. Electrochemical carbonization offers several advantages and limitations. One advantage of this technique is that it can produce CQDs with controlled size and surface chemistry, which can be tailored to specific applications in fields such as sensing and energy. Additionally, electrochemical carbonization is a relatively simple and low-cost method compared to other bottom-up methods, making it accessible to a wide range of researchers. However, it also has some limitations, including the need for careful control of the electrochemical conditions to ensure the production of high-quality CQDs with desired properties. In addition, the scalability of the technique may be limited by the need for specialized equipment and the potential for batch-to-batch variation in the resulting CQDs. Yuxin Hou and partners have proposed the synthesis of water-soluble functionalized fluorescent carbon dots through electrochemical carbonization of sodium citrate and urea for label-free sensing probe for selective detection of Hg^{2+}ions [46].

Hydrothermal/Solvothermal Synthesis

The techniques of hydrothermal/solvothermal synthesis are frequently utilized to create CQDs. High temperature and high pressure are used in these techniques to encourage the development of CQDs. While solvothermal synthesis uses organic solvents, hydrothermal synthesis conducts the reaction in an aqueous medium. One of the main advantages of these techniques is their ability to produce CQDs with a narrow size distribution and high quantum yields. Moreover, they can be easily scaled up for mass production. However, the main drawback of these techniques is the prolonged reaction times needed to produce CQDs.

For instance, Nammahackak et al. has produced CQDs with size tunability via heterogeneous nucleation in a hydrothermal synthesis process [47]. Other research conducted by Pang and his collaborators, shows a growing topic as high-performance nitrogen-doped CQDs for metal ion nanosensing and cell imaging. They based their synthesis on the

ethanol solvothermal process from lignin. Obtaining CQDs with uniform particle size, high quantum yield, and fluorescence stability. Furthermore, these CQD particles showed excellent biocompatibility and multicolored cell imaging ability [48]. Zhang and co-workers reported a one-step solvothermal treatment to synthesize pure red emissive CDs from citric acid and urea in formic acid without complicated purification procedures. They proved that the high content of C$\Longrightarrow$O groups contributes to their pure red emission. The enhanced single and multi-photon red fluorescence and enlarged particle sizes after surface modification with bovine serum albumin allowed the observation of in vivo tumor imaging and two-photon fluorescence imaging of blood vessels in mouse ears. [49].

Microwave Irradiation Synthesis

Microwave irradiation synthesis is a quick, clean, and low-cost synthesis method that is a sustainable method identified with the Green Chemistry demands [50]. It involves the use of microwave radiation to promote the formation of CQDs. One of the main advantages of microwave irradiation synthesis is its ability to produce CQDs with a high yield and relatively short reaction times compared to hydrothermal or solvothermal techniques. This technique also enables the facile control of the size and surface chemistry of the CQDs. However, the main disadvantage of microwave irradiation synthesis is the potential for overheating and carbonization of the reaction mixture if not carefully controlled. In 2012, Mitra et al. produced spherical CDs from poloxamer with a simple microwave-assisted process. The CDs exhibited bright blue and green fluorescent light under different excitation wavelengths. They suggested the use of these nanoparticles to fabricate fluorescent hydrophobic surfaces with excellent water resistance [21]. Highly fluorescent CDs prepared through this technique can be used for sensing devices due to the large amount of carboxyl and hydroxyl groups (-COOH and -OH) on the surface of the CDs, these features convert them into good candidates for monitoring $Cu2^{+}$ in environmental water samples [51].

Combining microwave irradiation synthesis with hydrothermal/solvothermal techniques can offer several advantages for the synthesis of CQDs. One of the main advantages is the potential to overcome the limitations. For example, although microwave irradiation synthesis can produce CQDs in a shorter period, it can also lead to overheating and carbonization if not carefully controlled. On the other hand, hydrothermal or solvothermal techniques can produce CQDs with narrow size distribution and high quantum yield, but they require long reaction times. Combining them can result in the production of CQDs

with improved size and optical features while also reducing the reaction time required.

Another advantage of combining these techniques is the potential to control the morphology and surface chemistry of the CQDs. Microwave irradiation can promote the formation of small CQDs with a high degree of crystallinity, while hydrothermal or solvothermal techniques can facilitate the functionalization of the CQD surface with various organic or inorganic molecules. This can enhance the stability and biocompatibility of the CQDs, making them more suitable for biological and medical applications. Hagiwara and collaborators successfully combined the microwave-solvothermal technique to obtain monodispersed CQDs. They reported the synthesis of yellow luminescent particles whose surface was functionalized with polyethylene glycol. These CQD particles showed higher quantum yields and possible bioapplications. In the study, they compared the new approach of microwave-solvothermal synthesis with conventional solvothermal synthesis, showing interesting improvements [52].

In addition, many other techniques can be classified as bottom-up or top-down techniques. Among them, arc discharge, plasma reactor, ultrasonic synthesis, chemical exfoliation, and combustion, metal-organic framework template-assisted approach, and others can be distinguished. Each technique has its characteristics, methodologies, precursors, and other parameters that lead to advantages or disadvantages depending on the objective of the research. Since the work's goal is not to analyze the different techniques for CQDs synthesis, the previously mentioned techniques will not be discussed in detail.

2.3 Surface Modification of CQDs

The properties of CQDs' can be further fine-tuned by surface modification. Modification can occur during or after synthesis by chemical or physical pathways [53]. These processes have a direct effect on the properties. There are three issues related to the synthesis of CQDs to be considered: 1) carbon particle aggregation, 2) uniformity and size control, and 3) surface properties of CQDs, which are critical for solubility and downstream applications. The first problem can be solved by electrochemical synthesis, confined pyrolysis, or chemical methods. Particle size can be controlled by further treatment by gel electrophoresis, centrifugation, or dialysis. And the surface area can be adjusted during or after the preparation of the CQDs [2].

2.3.1 Dopping

Doping is a method of tuning the photoluminescent properties of CQDs. Doping can consist of the incorporation of various heteroatoms, such as nitrogen, sulfur, phosphorus, or other elements, into the carbon structure. The modification offers several advantages, such as increased quantum yield (QY), shifted peak emission wavelengths, improved stability, and improved functionalities [2, 54, 55].

One of the primary advantages of CQDs doping with heteroatoms is the significant improvement in quantum yield. Quantum yield refers to the efficiency with which a quantum dot can emit light upon excitation. By introducing heteroatoms, the energy levels and electronic structure of the CQDs can be modified, leading to a more efficient radiative recombination process and higher QY [37, 41]. Nitrogen doping, in particular, has been widely studied and has demonstrated a substantial enhancement in the quantum yield of CQDs [36, 39].

Doping can also induce a shift in the emission peaks of CQDs. The emission wavelength of CQDs highly depends on its size and surface functionalization. By introducing heteroatoms, the energy levels within the CQDs can be adjusted, resulting in a shift of the emission peaks. This tunability enables the customization of CQDs for specific applications, such as fluorescence imaging, bioimaging, or optoelectronics [56]. For instance, Yang et al. used doped CQDs with ZnS salt in an in-vivo study for optical imaging. ZnS-doped particles enhanced their fluorescence producing a redshift [57].

2.3.2 Funtionalization

Structural tuning in the surface of the CQDs may allow further manipulation of their properties. For example, increasing biocompatibility [58], targeting [59], and stabilization (which is essential for biological applications as they are mainly stabilized by electrostatic interactions), changing optical properties, increasing/decreasing hydrophobicity, and surface charge [53].

Hydrophobic Effect

The hydrophobicity of CQDs plays a significant role in their behavior and potential applications. Hydrophobic CQDs have a low affinity for water, making them insoluble or poorly dispersible in aqueous environments. Hydrophobic CQDs enhance their stability in

organic solvents or nonpolar matrices. The hydrophobic surface of CQDs can prevent unwanted interactions with water molecules, minimizing aggregation and maintaining their structural integrity. This stability is particularly advantageous for applications that require CQDs to be incorporated into hydrophobic materials, such as polymer composites or organic coatings [60]. Additionally, hydrophobic CQDs can exhibit improved photoluminescence properties due to reduced surface quenching effects, resulting in brighter and more efficient fluorescence. However, the hydrophobicity of CQDs can also limit their utility in certain applications that require water compatibility or biocompatibility. For instance, hydrophilic CQDs are often preferred in bioimaging or biomedical applications due to their better dispersibility in aqueous solutions, reduced cytotoxicity, and enhanced biocompatibility. Hydrophilic CQDs can be achieved through surface functionalization with hydrophilic groups or by modifying the surface chemistry to increase water solubility [53, 61].

Surface Charge Effect

The surface charge of CQDs affects their dispersibility in various solvents and their interactions with biomolecules or other charged molecules. Anionic CQDs tend to have better dispersibility in polar solvents and aqueous environments due to repulsion between negatively charged particles [62]. On the other hand, a cationic CQD with its positive charges can facilitate interactions with negatively charged biomolecules or cellular membranes, enabling targeted delivery or specific binding in biological systems [63, 64]. The surface charge of CQDs can also influence their stability, aggregation behavior, and colloidal properties, thereby impacting their overall performance in various applications [65].

It's worth noting that the surface charge of CQDs can be modulated by adjusting the pH of the surrounding medium. At different pH values, the protonation or deprotonation of surface functional groups can alter the net charge of CQDs. This pH-dependent surface charge can be leveraged for pH-responsive drug delivery systems or sensing platforms. Mondal et al. developed citric acid-based CQDs for pH sensing and detection of Cr(VI) with excellent selectivity and sensibility. These CQDs were doped with lanthanide ions to improve their optical properties [66]. Overall, the surface charge of CQDs plays a crucial role in their dispersibility, interactions, and applications, making it an essential consideration in their design and synthesis.

Surface Passivation and Functionalization

Physical surface modification techniques include surface passivation. Through weak interactions such as van der Waals forces, *pi-pi* stacking, or hydrogen bonds, molecules or polymers are adsorbing or encapsulating on the surface of CQDs. With this approach, functional molecules can be attached to CQDs without changing their cores. The surface of CQDs can be passivated using organic molecules or polymers, which form a protective layer around the CQDs, shielding them from external influences. Passivation agents can act as surface ligands, providing steric hindrance and preventing the aggregation of CQDs [67]. Srivastava et al. passivated the surface of CDs with electron-acceptor and electron-donor groups and tested their photophysical properties both in bulk state and at the single-particle level [68].

The chemical surface modification involves functionalizing the surface of CQDs with different chemical groups or molecules. Functionalization involves attaching specific chemical groups or molecules (typically involves the attachment of functional groups, such as amino (-NH2), carboxyl (-COOH), hydroxyl (-OH), or thiol (-SH) groups) to the surface of CQDs, imparting desired properties and enhancing stability. Functional groups can provide electrostatic stabilization by introducing charges that repel each other, preventing aggregation [40]. Passivation and functionalization help to reduce surface defects, enhance photostability, and improve the dispersibility of CQDs in different solvents.

Chapter 3

Methodology

This chapter reviews in detail the experimental procedure that was performed to obtain and characterize the modified CQD particles.

3.1 Materials

Citric acid monohydrate (*VWR BDH Chemicals*) and urea (*Sigma-Aldrich*) were used as carbon and nitrogen sources, respectively. Dimethylformamide (DMF) (*VWR BDH Chemicals*) was used as the solvent for the synthesis of the CQDs. Dimethylsulfoxide (DMSO) (*Duchefa Biomedicals*), and distilled water were used as solvents. N-(3-dimethylaminopropyl)-N'-ethylcarbodiimide hydrochloride (EDC) (*Sigma-Aldrich*), 1-Hydroxybenzotriazole hydrate (HOBt) (*Sigma-Aldrich*), ethylenediamine (EDA) (*Sigma-Aldrich*), polyethyleneimine (PEI) (*Sigma-Aldrich*), and ethanolamine hydrochloride (ETA) (*Thermo Fisher*) were used for the surface modification of the CQDs.

3.1.1 Technical Data of the Reagents

Compound	Chemical formula	Molecular weight $gmol^{-1}$
DMF	C_3H_7NO	73.09
DMSO	C_2H_6OS	78.13
HOBt	$C_6H_5N_3O$	135.12
EDA	$C_2H_8N_2$	60.1
EDC	$C_8H_{17}N_3$	191.7
PEI	C_2H_5N	43.069
ETA	C_2H_7NO	61.08

Table 3.1: Technical data of the reagents.

3.2 Preparation of CQDs

3.2.1 Synthesis and Purification

The synthesis of the CQD particles was performed in a microwave-assisted reactor (CEM Discover SP). The reactor parameters were set at 200 °C, 4 h duration, 12 W of maximum power, and a pressure limit of 12 bar. Different batches of stock solution were prepared according to the requirements for the tests, based on the following amounts 2.5 mmole urea and 2 mmole citric acid were dissolved in 20 mL DMF. After the reaction, a dark solution was obtained and purified by dialysis for 24 h agains 2 L distilled water using 1 kDa porous membrane made of regenerated cellulose. The distilled water was replaced 3 times. After the purification process, the CQD batches were put in a rotary evaporator for drying to determine the dry mass and reaction yields. The product was redispersed in water at 10 g/L concentration and stored at 4 °C in a fridge.

3.2.2 Surface Modification

Several reagents at different concentrations were used for chemical and physical modification. Three main groups can be distinguished: 1) EDA-modified CQDs, 2) EDA-ETA-modified CQDs, and 3) PEI-modified CQDs. Tables 3.2, 3.3, and 3.4 summarizes the reagents and concentrations used for each modification. The reagents for each sample were dissolved in 5 mL of water. They were then left to stir overnight with the exception of the physical modification samples. These samples were left stirring for about 4h. Importantly, each CQD modification was followed by a purification process, rotary

evaporation, and mass yield determination. Samples were redispersed in water at 1 g/L concentration. Hereafter, the nomenclature CM# and PM# will be used to refer to the chemical or physical modification.

Chemical modification

To prepare the EDA series samples, the steps were as follows: 1) 50 mg of CQDs were dissolved in 2 mL of water; 2) the HOBt and EDC were dissolved in 1 mL of water each; 3) the solution of HOBt and EDC was added to the CQDs solution; 4) EDA was added with a micropipette and water was filled to complete 5 mL. In the case of CM4 sample EDA was replaced with PEI. In addition, the pH of samples CM2, CM3, and CM4 was determined and adjusted before the reaction started.

Sample	**CQD** mg	**HOBt** mg	**EDC** mg	**EDA** μL	**PEI** mg	**pH**
CM1	53	41.6	115.5	50	-	-
CM2	48.2	41.4	115.9	165	-	5.85
CM3	50.2	123.3	345.3	165	-	6.00
CM4	50.1	41.3	115.7	-	451.7	5.83

Table 3.2: Chemical modification of CQDs with EDA.

EDA-ETA series samples were prepared as follows: 1) the HOBt was dissolved in 2 mL of a 10 g/L solution of CQDs; 2) the EDC and ETA were dissolved in 1 mL of water each; 3) the EDA was poured with a micropipette and mixed into the ETA solution; 4) the EDC solution was poured into the HOBt-CQD mixture; 5) finally, the EDA-ETA was poured into the "stock" mixture and the volume was completed with water to 5 mL. Sample CM10 contains PEI instead of EDA-ETA.

Sample	**CQD** mL	**HOBt** mg	**EDC** mg	**EDA** μL	**ETA** mg	**PEI** mg
CM5	2	19.7	46.2	20	0	-
CM6	2	19.8	46.4	15	7.5	-
CM7	2	19.9	46.7	10	14.7	-
CM8	2	19.7	46.2	5	22.1	-
CM9	2	19.8	46.2	-	29.1	-
CM10	2	19.9	46.5	-	-	18.15

Table 3.3: Chemical modification of CQDs with EDA-ETA.

Physical modification

The physical modification was carried out by means of an adsorption process using PEI. For this purpose, to 2 mL of a 10 g/L solution of CQDs, a certain amount of PEI was added. The pH of samples PM4 and PM5 was adjusted to 4 and 10 with a concentrated solution of hydrochloric acid.

Sample	CQD mL	PEI mg	pH
PM1	2	15.2	-
PM2	2	150.6	-
PM3	2	450.1	-
PM4	2	150.1	4
PM5	2	150.3	10

Table 3.4: Physical modification of CQDs with PEI.

3.3 Characterization of Carbon Quantum Dots

3.3.1 Particle Size Determination

The dynamic light scattering (DLS) measurements were carried out with an LSI Nanolab 3D (LS Instruments, Switzerland). DLS system operating in 3D cross-correlation mode. As a light source, a fiber-coupled diode laser operating at 638 nm was used. The measurements above were performed at a detection angle of 90° at 25 °C. The measured autocorrelation functions were analyzed using the Corenn algorithm to determine the hydrodynamic radii of the particles.

3.3.2 Electrophoretic Mobility Properties

Electrophoretic mobility of the CQDs was determined in a Malvern Zetasizer Nano Z device at 25 °C. The average zeta potentials (ζ) were calculated from the mobility values using the Smoluchowski approximation.

3.3.3 Chemical Analysis of CQDs

An investigation of the chemical structure of CQD particles was carried out using attenuated total reflection infrared spectroscopy (ATR-IR) with a Jasco FT/IR-4x spectropho-

tometer from Japan. The ATR-IR measurements were performed with a resolution of 4 cm^{-1}, and 128 scans were obtained for each sample. Subsequently, the measured ATR-IR spectra were transformed to resemble Fourier transform infrared (FT-IR) spectra obtained in transmission mode using the instrument's SpectraAnalysis program. The positions and shapes of the peaks derived from the transformed ATR-IR spectra were compared with the results of FT-IR measurements documented in the literature.

3.3.4 Optical Properties

The optical properties were studied using two techniques: UV-Vis spectroscopy, and fluorescence spectroscopy. From UV-Vis spectroscopy (Analytic Jena, Specord 40), the absorption peak of the CQDs samples was determined. The concentration of the samples was kept in a range in which the absorbance was around 0.1. The fluorescence spectrophotometer (Varian Cary Eclipse fluorescence spectrophotometer) was used to record the excitation-emission 3D spectra of the samples. The 3D spectra were used to determine the excitation and emission wavelengths of the main fluorescence peaks. Fixed excitation wavelength (245, 350, 365, and 450 nm) 2D spectra were also recorded for a dilution series of the samples. These data were used in the calculations of the quantum yields, where quinine sulfate at several concentrations in 0.5 M H_2SO_4 was used as a standard.

Chapter 4

Experimental Results and Discussion

4.1 Synthesis and Purification

CQD particles were successfully synthesized through a microwave-assisted reaction with citric acid and urea as precursors in a DMF medium. DMF was chosen as the solvent because it can dissolve a wide range of both organic and inorganic compounds, it has a high polarity, good synthetic value up to high temperatures, and good thermal stability (even at the boiling point of 153°C) [69]. After the reaction, the colorless solution turned into a dark solution. The Tyndall effect was observed by using a laser. The purification process was carried out employing a dialysis process with a porous membrane of 1 kDa. The process allows the DMF solvent to be removed and exchanged for distilled water. Moreover, the purification process allows the removal of the unreacted molecules and to obtain pure CQDs. Special care was taken with the length of the membrane and the amount of solution poured into it, as the osmotic pressure increased as time elapsed. It could be suggested that the purification process be carried out by means of size exclusion chromatography to fine-tune the CQDs' size. In addition, the species with the highest fluorescence could be separated and concentrated into specific fractions [18].

After the purification process, the CQDs suspension was put in a rotary evaporator to dry the samples. A brownish material was obtained after the drying. The material was weighed and redispersed to get a 10 g/L solution. Table 4.1 summarizes the reaction yields of the prepared batches. The yield was calculated from the total amount of urea and citric acid used for each batch. It is observed that the higher the mass of the precursors, the higher the

reaction yield. This is something to take into consideration with the purification process, some material could be lost due to the manipulation of the raw CDQs, the manipulation of the membranes, and other factors that interfere with the yield.

	Citric Acid	**Urea**	**DMF**	**CQD**	**Yield**
	g	g	mL	g	%
Batch 1	8.4071	3.0045	400	0.4607	4.04
Batch 2	5.0441	1.8038	240	0.1897	2.77
Batch 3	2.1011	2.8519	100	0.0555	1.95

Table 4.1: Raw CQD yield. *Density: $0.95 kgL^{-1}$

4.2 Surface Modification

As previously described, the surface modification of the CQDs was performed by chemical and physical processing. Both procedures followed the same treatment as the raw CQDs (purification, rotary evaporation, reaction yield determination, redispersion of particles in water, and storage). EDC was used because it is a cross-linking agent that acts by activating carboxylic acid groups, which allows them to react with amine-containing molecules. EDC was combined with HOBt because it is a coupling reagent that increases the efficiency of the reaction by stabilizing the intermediate species formed during the coupling process [70]. In this study, EDA, ETA, and PEI were used as agents having amine groups in their structure. EDA is a type of diamine that contains two amine groups (-NH2). ETA contains one amine group (-NH2) and one hydroxyl group (-OH). And PEI is a polymer with repeating units of the amine-containing monomer ethyleneimine.

In the EDA series (CM1 to CM3), sample CM1 is used as a control sample. Samples CM2 and CM3 contain three times the amount of EDA used in sample CM1. In addition, sample CM3 contains three times the amount of EDC and HOBt. In the EDA-ETA series (CM5 to CM9), the EDA concentration decreases as the ETA concentration increases. Finally, in the PEI series (CM4, CM10, PM1 to PM5) 3 groups are distinguished in terms of PEI concentration: 1) CM4 and PM3 (450 mg PEI), 2) PM2, 4 and 5 (150 mg PEI), and 3) PM1 (15 mg PEI). This description will help the reader to better interpret and read the results obtained.

The physical and chemical modifications resulted in a liquid phase and the formation of a precipitate. The precipitate can be attributed to the particle's aggregation after the treatment, probably due to physical aggregation as well as chemical cross-linking by the bifunctional EDA and multifunctional PEI. Table 4.2 summarizes the yield of each sample and whether or not a precipitate was obtained after modification. To determine the yield, the liquid part was separated from the solid part by centrifugation. The liquid part was put under rotational evaporation and the product was weighed. The precipitate was also dried and weighed. The product of the liquid phase was redissolved in distilled water at a concentration of 1 g/L. The precipitate was subjected to solubility tests with different solvents. DMSO was the only solvent capable of solubilizing the precipitate. Furthermore, one of the precipitates was added diluted solutions of HCl and NaOH to decrease and increase the pH. The precipitate started to solubilize when the pH reached a value of around 11. It is important to note that the precipitate yield is not recorded for samples CM1 to CM4, as these were used for the solubility tests. However, it is estimated that the mass of the precipitate of these samples is similar to the others obtained. No precipitate was formed insamples CM10, PM2, and PM3. It is observed that from the 20 mg of raw CQDs used for the modifications, yields were obtained between 7.5 to 46.5%.

Sample	**LP** mg	**P** mg	**LP Yield** %	**P Yield** %	**LP + P Yield** %
CM1	2.9	-	14.5	-	14.5
CM2	3.2	-	16	-	16
CM3	5.6	-	28	-	28
CM5	3.7	0.3	18.5	1.5	20
CM6	1.9	0.4	9.5	2	11.5
CM7	4.4	0.7	22	3.5	25.5
CM8	9.2	0.9	46	4.5	50.5
CM9	2.5	0.9	12.5	4.5	17
CM4	3.8	-	19	-	19
CM10	3.3	-	16.5	-	16.5
PM1	4.7	0.3	23.5	1.5	25
PM2	9.3	-	46.5	-	46.5
PM3	1.5	-	7.5	-	7.5
PM4	4.3	1.1	21.5	5.5	27
PM5	2.3	0.5	11.5	2.5	14

Table 4.2: Yield of the chemical and physical modifications. (LP: liquid phase, P: precipitate)

4.3 Particle Size and Electrophoretic Mobility Properties

DLS and electrophoretic mobility measurements are shown in Tables 4.3, 4.4 and 4.5 for the EDA, EDA-ETA, and PEI series, respectively. DLS measurements confirm the small size of the CQD particles. The hydrodynamic diameter determined by DLS takes into account both the particle's physical size and the solvent molecules that surround it and form a dynamic layer around it known as the "hydration shell" or "diffuse layer." Due to numerous interactions including electrostatic forces, van der Waals forces, or steric effects, the solvent molecules in this layer are closely bound to the surface of the particle [71].

DLS measurements were not performed for the EDA series since the CM5 sample only contains EDA. In the same way, the DLS experiment was carried out only for the sample PM3 since the other samples in that series only differ in the amount/concentration of PEI reagent. The hydrodynamic diameters for the studied samples are below 12.5 nm. The untreated CQD particles show a diameter of (4.08 $\pm$ 0.03) nm. All samples showed a low polydispersity. The polydispersity was calculated by dividing the standard deviation by the mean hydrodynamic diameter and then squaring up this result. Low polydispersity is preferable since it indicates a population of particles with uniform sizes. It is observed that the diameter of particles containing PEI (CM10 and PM3) are approximately the same. In the EDA-ETA series, there is no obvious trend in particle diameter. However, the largest value is attributed to sample CM7. The differences in size could be explained by electrostatic interactions between the surface groups of the CQDs. As the modification proceeds the carboxyl groups are partially consumed. This means a reduction in the number of negative charges and an overall shift to a smaller net charge that can result in decreased electrostatic interactions and consequently aggregation. Furthermore, the size increase can also be attributed to the chemical cross-linking between the particles. In addition, it should be noted that DLS is an excellent technique for determining approximate particle size, however, the QCD size is at the lower limit of sensitivity of this technique. It can be recommended to use atomic force microscopy (AFM) and scanning electron microscopy (SEM) characterization to better determine the particle size of QCDs.

Sample	DLS Diameter nm	SD	Polydispersity $\times 10^{-5}$ / nm^{-2}	Electrophoretic mobility Zeta Potential mV	SD
CQD	4.08	0.03	5.96	-30.3	2.4
CM1	-	-	-	-1.8	0.6
CM2	-	-	-	-9.5	0.2
CM3	-	-	-	-6.5	0.7

Table 4.3: DLS and electrophoretic mobility measurements for the EDA series.

Sample	DLS Diameter nm	SD	Polydispersity $\times 10^{-5}$ / nm^{-2}	Electrophoretic mobility Zeta Potential mV	SD
CM5	8.14	0.03	1.36	-3.0	0.5
CM6	11.88	0.03	0.73	-2.6	0.3
CM7	12.48	0.03	0.58	-4.3	0.2
CM8	7.38	0.03	2.11	-7.5	1.2
CM9	9.93	0.03	0.98	-11.1	0.9

Table 4.4: DLS and electrophoretic mobility measurements for the EDA-ETA series.

Sample	DLS Diameter nm	SD	Polydispersity $\times 10^{-5}$ / nm^{-2}	Electrophoretic mobility Zeta Potential mV	SD
CM4	-	-	-	5.8	1.2
CM10	1.68	0.03	34.1	8.4	3.2
PM1	-	-	-	1.9	1.4
PM2	-	-	-	6.7	4.3
PM3	2.54	0.04	20.2	1.4	0.4
PM4	-	-	-	10.1	5.1
PM5	-	-	-	3.3	1.2

Table 4.5: DLS and electrophoretic mobility measurements for the PEI series.

The study of electrophoretic mobility of CQD particles entails monitoring the velocity of the particles under the influence of an applied electric field. This method is used to evaluate the stability and surface charge of the particles in a solution. The zeta potential analysis is an important aspect of electrophoretic mobility studies. A high absolute value of zeta potential (positive or negative) indicates the existence of strong repulsive forces between the particles, which increases stability and decreases aggregation. On the other hand, a low absolute value of zeta potential, close to zero, denotes weak repulsion, which makes

the particles more susceptible to aggregation and precipitation. The pH is an important factor that can affect the zeta potential. [72]. There are other factors that can affect the zeta potential such as conductivity and ion concentration. However, these aspects will not be discussed further.

The unmodified CQDs exhibit a zeta potential of (-30.1 ± 2.4) mV. For such small particles, this is a relatively high value, that is responsible for the long-term stability of the system. The modified CQDs display values are ranging from -11 to 10 mV. In the EDA and EDA-ETA series, negative zeta potential values are observed, while the PEI series shows positive values for both types of modifications. The theory suggests that the functional groups of the untreated CQD sample are deprotonated, providing an explanation for the highly negative value and indicating the high stability of CQDs. However, the modifications with EDA, PEI, and EDA-ETA have a gradual shift toward positive zeta potential values compared to the raw CQDs, through the introduction of new positively charged amine groups, with the resulting net charge values approaching zero. This can reduce the electrostatically driven adsorption, which means that these particles are at their isoelectric point, reducing their stability and leading to the formation of aggregates. The aggregation of CQDs may account for the precipitates obtained in most of these samples. This is strengthened by the observation that above pH 11, where the amine groups become neutral, partial dissolution of the aggregates was seen. This can be explained that the net charge of the particles becomes more negative through the remaining deprotonated carboxyl groups.

Samples CM2 and CM3 were subjected to testing in an acidic environment with a pH of approximately 6. The key distinction between these two samples lies in their concentrations of HOBt and EDC. Analysis of the zeta potential results reveals a slight increase in their respective values. This suggests that sample CM3, with a higher concentration of coupling agents, facilitates a stronger coupling of EDA. In contrast, sample CM1 exhibits a zeta potential value closer to zero, indicating a balanced presence of carboxyl and amine groups.

The EDA-ETA series demonstrates an increasing trend in zeta potential values with respect to the ETA concentration. This indicates that a significant number of carboxylic groups remain following the reaction and also that the ETA conjugation is possibly less promoted. The chemically and physically modified PEI samples exhibit positive zeta po-

tential values. This is expected, as PEI contains numerous amine functionalities, with its binding the charge balance is more readily shifted to the positive range. Comparing CM4 and CM10, their zeta potential values display slight differences attributable to variations in PEI concentration. Increasing the concentration of PEI leads to two effects: an increase in the number of PEI molecules that can bond to the CQDs' surface, and an increase in the ionic strength of the solution. With increased ionic strength, the electrostatic interactions between the particle and polymer become more short-range, which can reduce the driving force of PEI adsorption. Since the first step of the chemical coupling is also the adsorption of the polymer molecule, this can affect the coupled polymer amount as well.

Regarding the physical modification, two interesting effects could be observed. PM1, PM2, and PM3 samples were prepared under the same conditions but with different PEI concentrations. A monotonous increase in the adsorbed amount was expected with increasing polymer concentration mirrored by a gradual shift toward positive values. Instead, maximum zeta potential can be seen with PM2. PEI being a polyelectrolyte increases the ionic strength of the medium quite significantly. This can reduce adsorption. The polymer also shifts the pH to the basic range at an increased concentration which can further reduce the number of protonated amine functional groups. To study the pH effect, physisorption was also carried out at controlled pH of 4 (PM4) and 10 (PM5) at the same concentration as PM2. Since measurements were carried out after dialysis the pH control during the preparation was not affecting the measured zeta potential values. When acidic conditions were used, where the amine groups of the PEI are protonated while the carboxylic groups of the CQDs are still deprotonated an increased zeta potential was achieved. Conversely at pH 10 where the charged character of PEI is less pronounced a smaller zeta potential modified particle could be generated. This indicates that the electrostatic interactions greatly influence the surface modification of the CQDs. In the case of PEI with careful optimization, the charge character of the particles can be fine-tuned.

4.4 Chemical Analysis of CQDs

Infrared spectroscopy was employed to investigate the chemical composition of CQDs. Notably, a prominent and broad peak was observed in the region of 2500-3700 cm^{-1} (4.1. A). This spectral region primarily corresponds to the stretching vibrations of OH and NH functional groups. Within this range, the asymmetric and symmetric C-H stretching

vibrations of CH_3 and CH_2 groups were identified at wavenumbers of 2970 cm^{-1} and 2936 cm^{-1}, respectively. Additionally, a distinct carboxylic OH stretching signal was observed at 2750 cm^{-1}. Upon conjugation, a decrease in intensity was observed in the lower wavenumber portion of the broad signal, suggesting the consumption of carboxylic groups. This decrease was particularly evident in the carboxylic OH vibrations. Furthermore, the carboxylic C=O stretching vibration was clearly observed at 1770 cm^{-1}, along with a broad peak centered around 1700 cm^{-1} in the unmodified CQDs spectrum (4.1. B). The peak at 1770 cm^{-1} is associated with the presence of monomeric carboxylic groups, while the peak at 1700 cm^{-1} is typically attributed to hydrogen-bonded dimeric carboxylic groups [73]. Both of these peaks were significantly reduced after the conjugation process. The latter peak also exhibited a shoulder at approximately 1680 cm^{-1}, which could be attributed to imid functional groups (C=O stretching) resulting from the citric acid-urea condensation reaction.

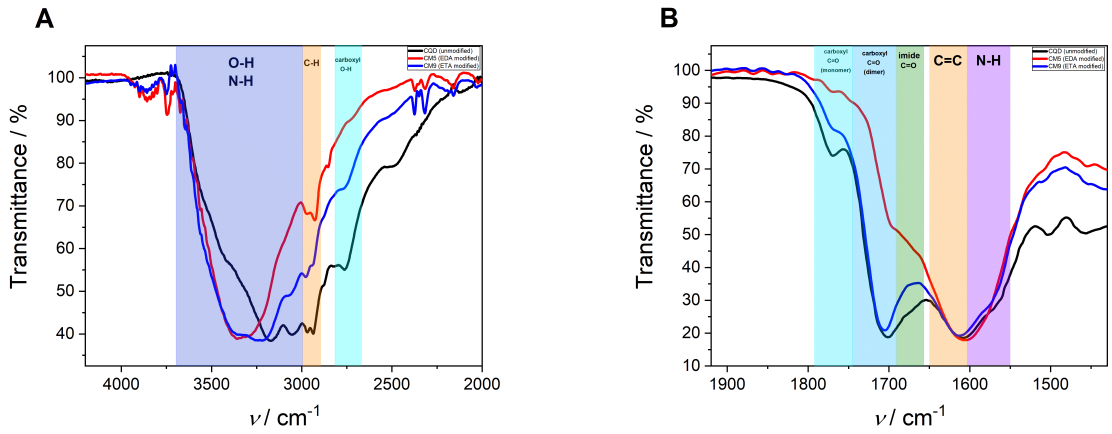

Figure 4.1: ATR-IR spectra of unmodified (black line), EDA modified (red line) and ETA modified (blue line) CQD samples in the 2000 to 4200 cm^{-1} (**A**) and 1430-1920 cm^{-1} (**B**) regions.

Another notable peak in this spectral region, occurring around 1600 cm^{-1}, displayed at least two distinct components. The first peak observed at approximately 1610 cm^{-1} was assigned to the conjugated C=O stretching of the particle core. The second prominent component, situated at around 1570 cm^{-1}, was attributed to N-H bending. Following ethylene-diamine conjugation, this peak was enhanced due to the introduction of new amine groups.

When ethanolamine was employed for the conjugation process, no significant changes in the shape of the spectrum within the 1650-1750 cm^{-1} range were observed. Only the peak

at 1770 cm^{-1}, corresponding to free carboxylic acid, exhibited a reduction in intensity. These results suggest that the coupling reaction using ethanolamine as a reagent was only partially successful.

4.5 Optical Properties

4.5.1 Fluorescence

The optical properties of the raw and modified CQDs were studied by UV-Vis and fluorescence spectroscopy techniques. Fluorescence is one of the most interesting properties of these types of particles. The fluorescence results are shown in the figures 4.2 4.3, 4.4, and 4.5, respectively. In general, the 3D fluorescence spectra show similarities between all of them in shape but differ in fluorescence intensity. Three peaks of high, medium, and low fluorescence can be distinguished. Two peaks in the emission range between 400 to 500 nm, and one peak above 500 nm emission range.

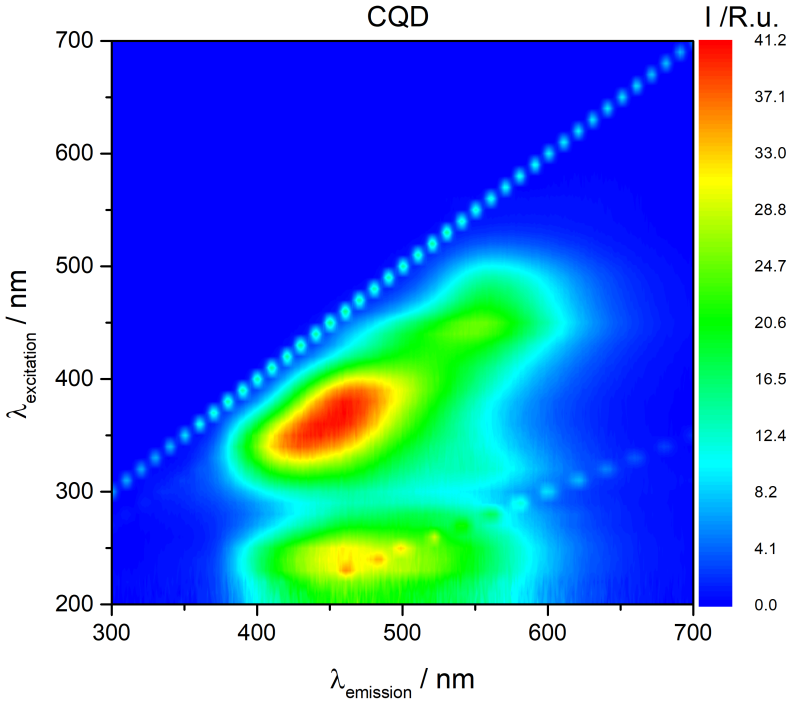

Figure 4.2: 3D fluorescence spectrum of unmodified CQDs.

Figure 4.2 shows the 3D fluorescence spectrum of the raw CQDs. It exhibited an intense excitation peak at around 375 nm corresponding with an emission wavelength of about 450 nm. A second peak (medium intensity) is found at an excitation wavelength of about

240 nm and the corresponding emission at about 450 nm. The third peak (low intensity) is located at around 450 nm excitation and 550 nm emission wavelengths. Table 4.6 summarizes the maximum excitation and emission peaks of the studied samples.

The Stokes shift, or bandgap, illustrated in Table 4.6, denotes the difference in wavelengths between fluorescence excitation and emission in CQDs. This phenomenon arises due to the energy losses, the energy levels of the absorbed photons are slightly higher than the emitted photons, leading to a Stocks shift or bandgap between the excitation and emission wavelengths. Notably, all the examined samples exhibited a consistent bandgap for the three peaks, highlighting the uniformity in this characteristic across the studied CQDs.

Sample		**Peak 1**			**Peak 2**			**Peak 3**		
		λ_{em}	λ_{ex}	**Bandgap**	λ_{em}	λ_{ex}	**Bandgap**	λ_{em}	λ_{ex}	**Bandgap**
		nm	nm	nm	nm	nm	nm	nm	nm	nm
Raw	**CQD**	464	238	226	460	375	85	548	449	99
EDA	**CM1**	473	243	230	463	377	86	549	443	106
	CM2	473	240	233	467	387	80	554	455	99
	CM3	477	241	236	468	382	86	547	446	101
EDA-ETA	**CM5**	473	237	236	467	386	81	546	450	96
	CM6	471	236	235	467	385	82	548	451	97
	CM7	470	237	233	466	384	82	543	449	94
	CM8	470	235	235	465	387	78	552	452	100
	CM9	469	236	233	466	385	81	554	452	102
PEI	**CM4**	470	237	233	469	383	86	551	450	101
	CM10	468	239	229	466	384	82	551	460	91
	PM3	460	249	211	462	379	83	550	456	94

Table 4.6: Maximum fluorescence peaks of the chemical and physical modifications of the CQDs.

The fluorescence phenomenon of CQDs is not fully understood. Based on previous work, the fluorescence peaks can be attributed to various luminescent centers present in the CQDs. The high-intensity peak can be associated with CQDs' π states related to sp^2-hybridized aromatic carbons. The region of the medium-intensity peak can be attributed to conjugated structures ($\pi \rightarrow \pi^*$ transitions) in the CQDs' core. And the low-intensity peak can be related to n $\rightarrow \pi^*$ transitions of surface functional groups of the particles.

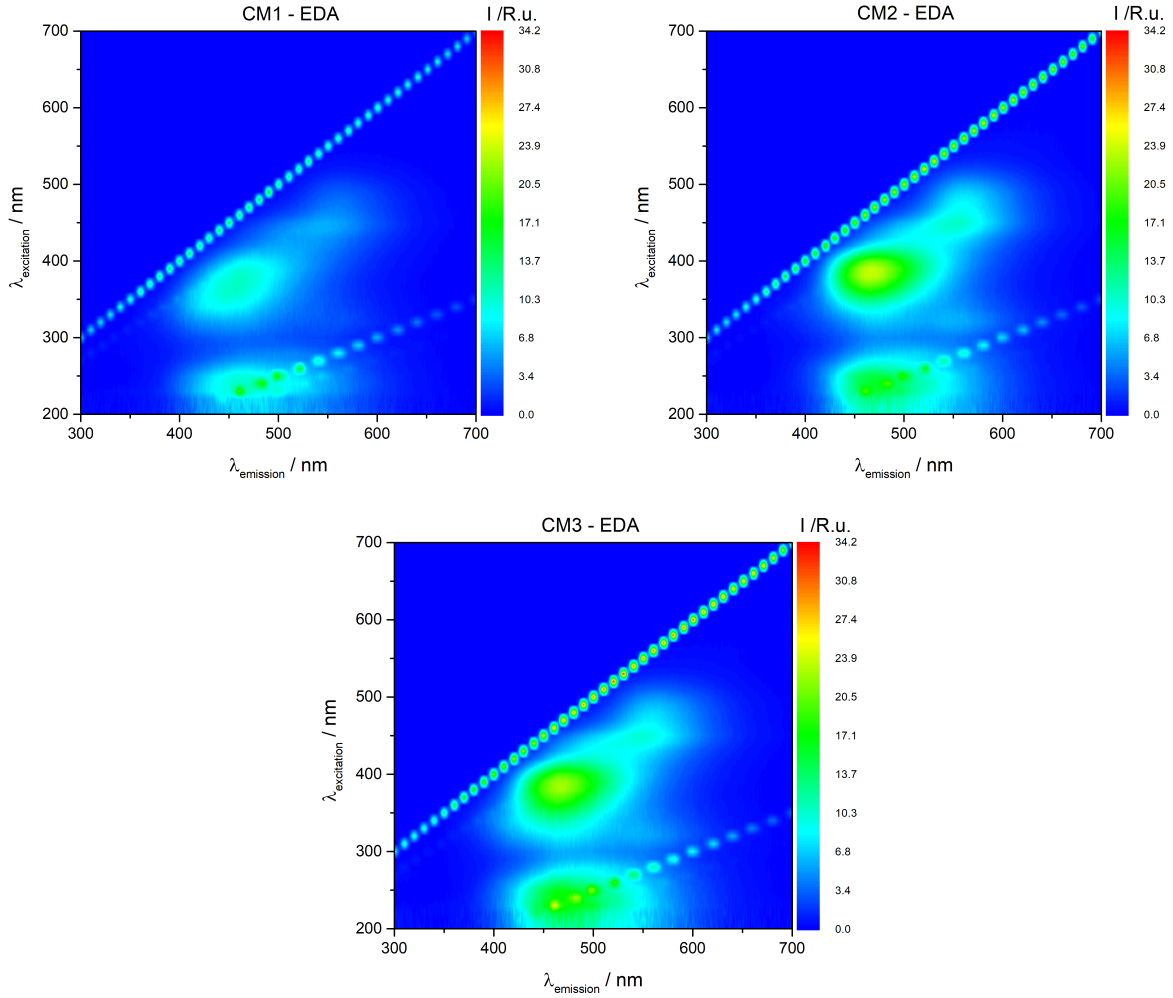

Figure 4.3: 3D fluorescence spectra of the chemical modification: EDA series.

Figures 4.3 and 4.4 show the 3D fluorescence spectra of the EDA and EDA-ETA series, respectively. Samples CM2 and CM3 present a higher-intense peak regarding the CM1 sample in the 475 nm emission range. The CM1 sample shows a barely visible fluorescence peak at the 550 nm emission region compared to the other two samples. On the other hand, the samples of the EDA-ETA series exhibit more intense peaks, especially the CM9 sample which only contains ETA. It is noticeable that as the ETA concentration increases also the fluorescence increases.

When the results from the IR measurements are also taken into account in general the following conclusion can be drawn. With conjugation the carboxylic content of the particles is reduced which is followed by a significant decrease in the measured fluorescence intensities, but no significant shifting in the spectral ranges. This indicates that the presence of the free carboxylic groups is essential in the fluorescence mechanism. Its exact

role however has to be further studied. This is also apparent with the ETA modification. According to the IR measurements following the ETA conjugation, a significant amount of carboxylic groups remain in the particles. The fluorescence seems to correlate well with this, as with increasing ETA concentrations the fluorescence intensities increased.

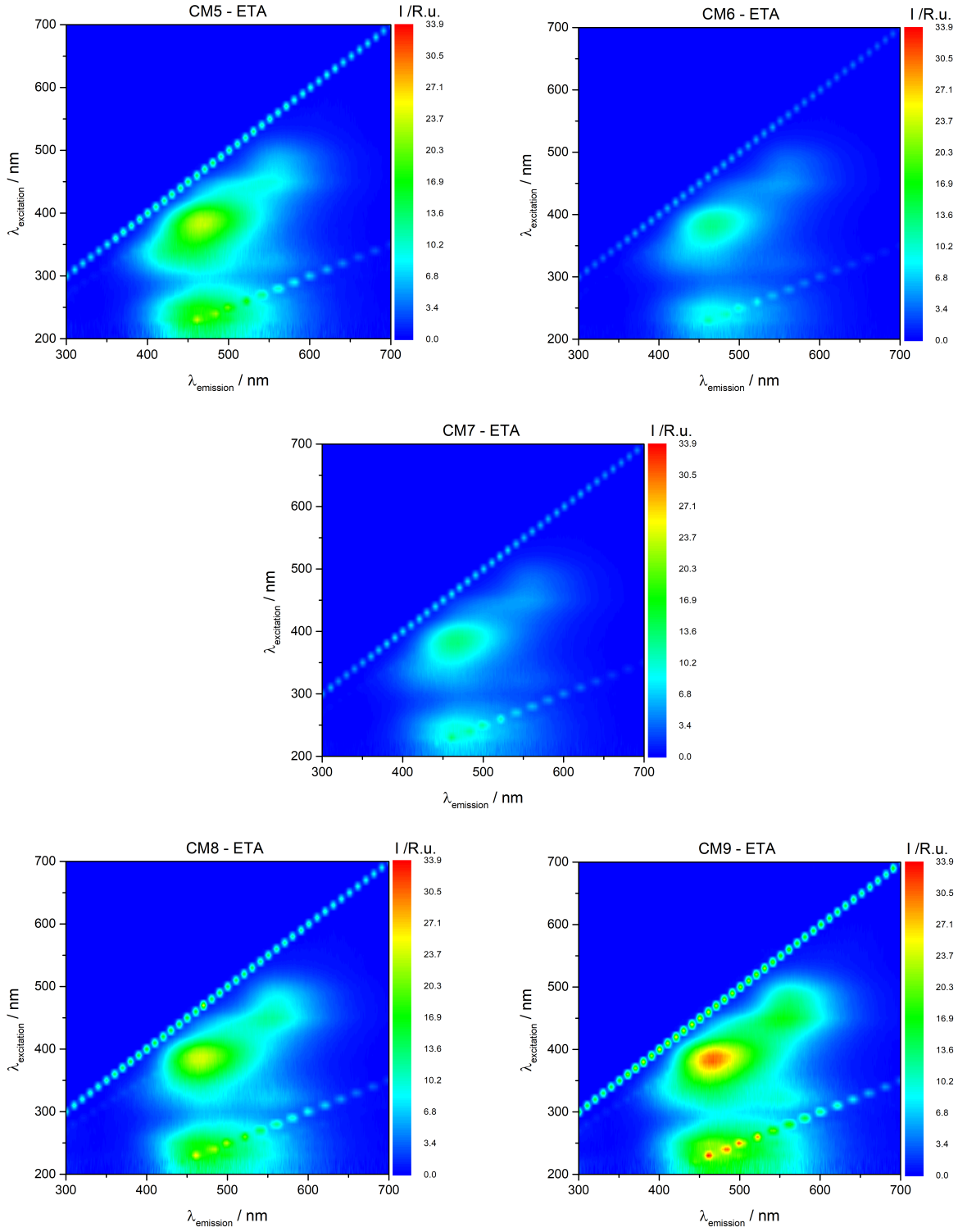

Figure 4.4: 3D fluorescence spectra of the chemical modification: EDA-ETA series.

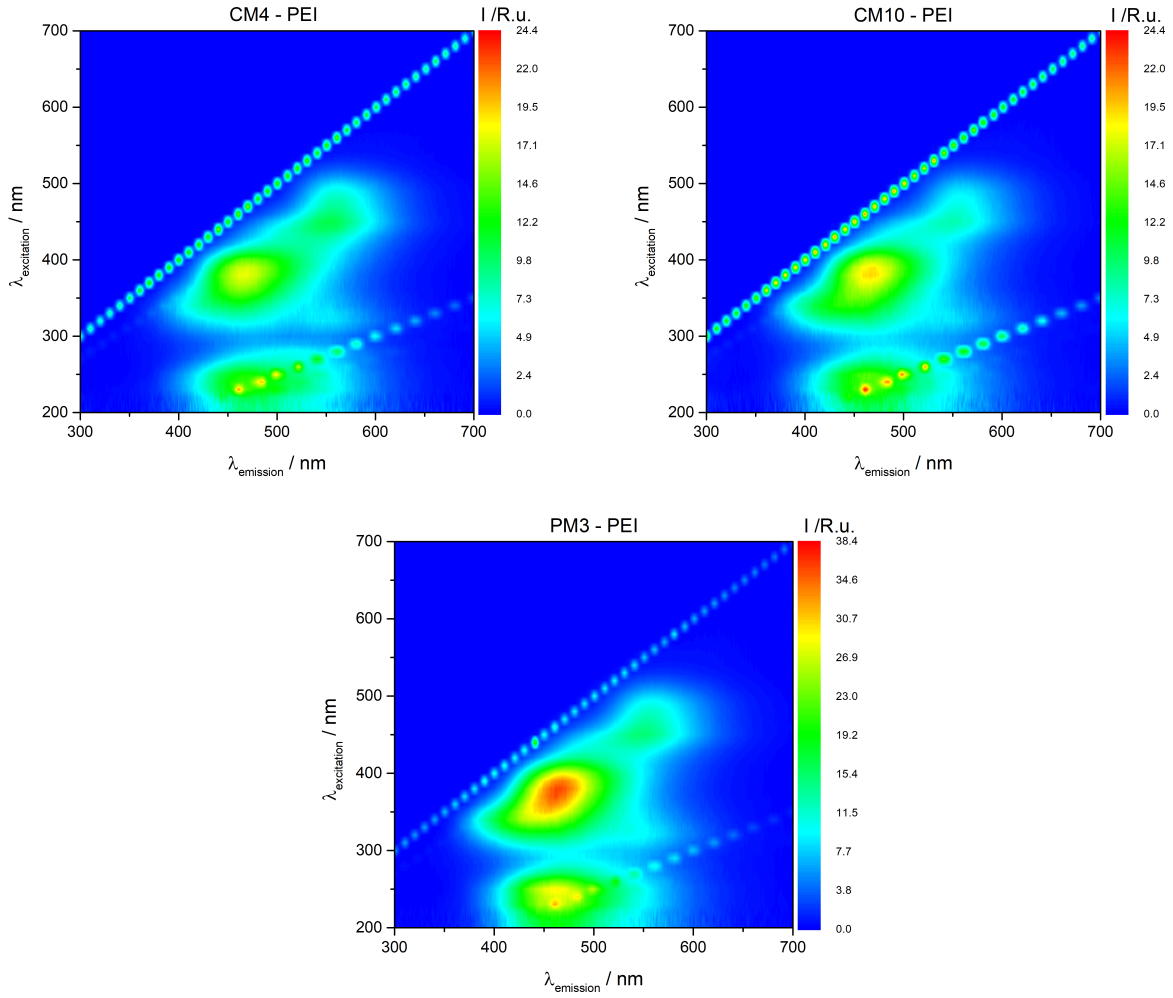

Figure 4.5: 3D fluorescence spectra of the chemical and physical modification: PEI series.

Figure 4.5 displays the 3D fluorescence spectra of the PEI series that corresponds with the physical and chemical modifications procedures. At first sight, the three spectra exhibit the same shape of fluorescence but different intensities regarding chemical and physical modification. Similarly to the EDA modification, chemically coupling PEI to the particles significantly reduces the fluorescence intensities. On the other hand, the physically modified PM3 sample shows much more intense fluorescence, probably due to not consuming the carboxylic groups of the CQDs. This leads to conclude that the physical modification shows better results in terms of photoluminescence properties. However, the maximum peak intensity is a bit lower than the raw CQDs, probably a result of strong electrostatic interactions between the ionized functional groups.

4.5.2 Quantum Yield

The compound quinine sulfate in 0.5 M H_2SO_4 solution was used as a reference to determine the quantum yield of the analyzed samples. This reagent is commonly used as a fluorescence reference standard. It has an absorbance peak at 350 nm, a refractive index of 1.33 at 25°C, and a well-known quantum yield of 0.54 (supporting information provided by Zhu and collaborators [74]). The quantum yield can be determined by equation 4.1 where Q is the quantum yield, m is the integrated fluorescence intensity against absorbance (gradient), and n is the refractive index of the solvents (s: studied sample and r: reference) [75].

$$Q_s = Q_r \left(\frac{m_s}{m_r}\right) \left(\frac{n_s}{n_r}\right)^2 \tag{4.1}$$

Bashkatov and Genina [76] developed a simple way to determine water refractive indexes at different temperatures and excitation wavelengths based on the Cauchy equation. They developed an approximation procedure to determine new temperature-dependent Cauchy coefficients. Equation 4.2 considered the Cauchy coefficients A, B, C, and D as a function of the temperature, and λ is the excitation wavelength in nm.

$$n(\lambda, T) = A\,(T) + \frac{B(T)}{\lambda^2} + \frac{C(T)}{\lambda^4} + \frac{D(T)}{\lambda^6} \tag{4.2}$$

Table 4.7 shows the Cauchy coefficients at 25 °C values used for the calculation of the quantum yield of the CQDs samples.

T °C	**A**	**B**	**C** $\times 10^8$	**D**
20	1.31984	5190.553	-2.56169	9.39388
30	1.31885	5173.866	-2.56817	9.43261
25	1.31935	5182.209	-2.56493	9.41325

Table 4.7: Cauchy coefficients for the determination of water refractive indexes at 25°C.

The response of four excitation wavelengths λ_{245}, λ_{350}, λ_{365}, and λ_{450} was measured. By using equation 4.2, the water refractive indexes values at λ_{245}, λ_{350}, λ_{365}, and λ_{450} were 1.334, 1.345, 1344, and 1.339, respectively. The values of m_s y m_r were determined by plotting the integrated fluorescence intensity against absorbance. By replacing the obtained

data into equation 4.2 it was obtained the QY for the different excitation wavelengths. Table 4.8 summarized the obtained values.

Sample		λ_{245}	λ_{350}	λ_{365}	λ_{450}
Raw	**CQD**	1.6	2.7	2.8	1.9
EDA	**CM1**	1.0	0.6	1.0	0.6
	CM2	1.0	0.8	1.2	0.8
	CM3	2.3	1.9	2.2	1.3
EDA-ETA	**CM5**	1.5	1.6	1.8	0.9
	CM6	0.7	0.8	0.8	0.5
	CM7	0.8	0.9	0.9	0.6
	CM8	1.0	0.9	1.1	0.8
	CM9	1.7	1.9	2.1	1.6
PEI	**CM4**	1.0	1.1	1.2	0.9
	CM10	1.4	1.6	1.7	0.9
	PM3	2.5	3.3	3.5	1.6

Table 4.8: Quantum yield of the chemical and physical modifications in percentage.

The quantum yields of unmodified CQDs were consistent with the reported values for the precursor couple citric acid/urea [77]. Generally, the chemically modified CQDs exhibited relatively lower QYs compared with the non-modified ones. Conversely, the physical modification of CQDs demonstrated superior results, indicating that physical modification may be the optimal approach for fine-tuning CQDs' properties. Nevertheless, this does not diminish the usefulness of chemical modification, as it provides a starting point for developing novel strategies to customize CQDs for biological applications where the goal is to introduce specific interactions with targeted cells.

Chapter 5

Conclusions

In conclusion, the synthesis of CQDs was successfully achieved, followed by their modification through chemical and physical processes. Binding agents HOBt and EDC, along with surface modifiers EDA, ETA, and PEI, were employed to modify the CQDs. Characterization experiments, including UV-Vis, fluorescence, and ATR-IR spectroscopy, provided valuable insights into the properties of the CQDs. The results confirmed the small size of the CQDs through DLS analysis. Zeta potential analysis supported the stability of the unmodified CQDs and the changes in surface charges following the modification process. Infrared spectroscopy played a crucial role in determining the chemical composition of the samples. The fluorescence experiments revealed consistent peaks in excitation and emission wavelengths, with variations observed mainly in peak intensity. The chemically modified samples exhibited lower quantum yield values compared to the physical ones, suggesting the potential for enhancing the quantum yield through fine-tuning of chemical modification parameters. These findings lay a solid foundation for future research, allowing for the exploration of alternative methodologies and the optimization of particle parameters for diverse applications in peptide modifications, bacterial membrane affinity, and polarity interactions with living membranes.

Bibliography

(1) Zhou, J.; Booker, C.; Li, R.; Zhou, X.; Sham, T. K.; Sun, X.; Ding, Z. *Journal of the American Chemical Society* **2007**, *129*, DOI: 10.1021/ja0669070.

(2) Wang, Y.; Hu, A. *Journal of Materials Chemistry C* **2014**, *2*, DOI: 10.1039/c4tc00988f.

(3) Lim, S. Y.; Shen, W.; Gao, Z. *Chemical Society Reviews* **2015**, *44*, DOI: 10.1039/c4cs00269e.

(4) Zhu, S.; Song, Y.; Zhao, X.; Shao, J.; Zhang, J.; Yang, B. *Nano Research* **2015**, *8*, DOI: 10.1007/s12274-014-0644-3.

(5) Li, S.; Li, L.; Tu, H.; Zhang, H.; Silvester, D.; Banks, C.; Zou, G.; Hou, H.; Ji, X. *Materials Today* **2021**, *51*, DOI: 10.1016/j.mattod.2021.07.028.

(6) Yazid, S. N. A. M.; Chin, S. F.; Pang, S. C.; Ng, S. M. *Microchimica Acta* **2013**, *180*, DOI: 10.1007/s00604-012-0908-0.

(7) Gupta, A.; Verma, N. C.; Khan, S.; Tiwari, S.; Chaudhary, A.; Nandi, C. K. *Sensors and Actuators, B: Chemical* **2016**, *232*, DOI: 10.1016/j.snb.2016.03.110.

(8) Liu, J.; Li, R.; Yang, B. *ACS Central Science* **2020**, *6*, DOI: 10.1021/acscentsci.0c01306.

(9) Lu, X.; Zhang, Z.; Xia, Q.; Hou, M.; Yan, C.; Chen, Z.; Xu, Y.; Liu, R. *Materials Science and Engineering C* **2018**, *82*, DOI: 10.1016/j.msec.2017.08.074.

(10) Gao, X.; Du, C.; Zhuang, Z.; Chen, W. *Journal of Materials Chemistry C* **2016**, *4*, DOI: 10.1039/c6tc02055k.

(11) Kwon, W.; Do, S.; Won, D. C.; Rhee, S. W. *ACS Applied Materials and Interfaces* **2013**, *5*, DOI: 10.1021/am3023898.

(12) Tang, Q.; Zhu, W.; He, B.; Yang, P. *ACS Nano* **2017**, *11*, DOI: 10.1021/acsnano.6b06867.

(13) Cui, B.; Feng, X. T.; Zhang, F.; Wang, Y. L.; Liu, X. G.; Yang, Y. Z.; Jia, H. S. *Xinxing Tan Cailiao/New Carbon Materials* **2017**, *32*, DOI: 10.1016/S1872-5805(17)60130-6.

(14) Baslak, C.; Demirel, S.; Kocyigit, A.; Alatli, H.; Yildirim, M. *Materials Science in Semiconductor Processing* **2022**, *147*, DOI: 10.1016/J.MSSP.2022.106738.

(15) Sahai, S.; Jangra, A.; Thomas, L. M.; Satsangi, V. R. *Journal of The Institution of Engineers (India): Series D* **2023**, DOI: 10.1007/s40033-023-00490-x.

(16) Xu, X.; Ray, R.; Gu, Y.; Ploehn, H.; Gearheart, L.; Raker, K.; Scrivens, W. *Journal of the American Chemical Society* **2004**, *126*, DOI: 10.1021/ja040082h.

(17) Sun, Y.-P.; Zhou, B.; Lin, Y.; Wang, W.; Fernando, K.; Pathak, P.; Meziani, M.; Harruff, B.; Wang, X.; Wang, H.; Veca, L.; Xie, S.-Y. *Journal of the American Chemical Society* **2006**, *128*, DOI: 10.1021/ja062677d.

(18) Giordano, M. G.; Seganti, G.; Bartoli, M.; Tagliaferro, A. *Molecules (Basel, Switzerland)* **2023**, *28*, DOI: 10.3390/molecules28062772.

(19) Bhattacharyya, S.; Ehrat, F.; Urban, P.; Teves, R.; Wyrwich, R.; Döblinger, M.; Feldmann, J.; Urban, A. S.; Stolarczyk, J. K. *Nature Communications* **2017**, *8*, DOI: 10.1038/s41467-017-01463-x.

(20) Mitra, S.; Chandra, S.; Pathan, S. H.; Sikdar, N.; Pramanik, P.; Goswami, A. *RSC Advances* **2013**, *3*, DOI: 10.1039/c2ra23085b.

(21) *RSC Advances* **2012**, *2*, DOI: 10.1039/c2ra21048g.

(22) Chandra, S.; Pathan, S. H.; Mitra, S.; Modha, B. H.; Goswami, A.; Pramanik, P. *RSC Advances* **2012**, *2*, DOI: 10.1039/c2ra00030j.

(23) Feng, X. T.; Zhang, F.; Wang, Y. L.; Zhang, Y.; Yang, Y. Z.; Liu, X. G. *Applied Physics Letters* **2015**, *107*, DOI: 10.1063/1.4936234.

(24) Yro, P. A. N. D.; Quaichon, G. M. O.; Cruz, R. A. T.; Emolaga, C. S.; Que, M. C. O.; Magdaluyo, E. J. R.; Basilia, B. A. *AIP Conference Proceedings* **2019**, *2083*, DOI: 10.1063/1.5094310.

(25) Zavareh, H. S.; Pourmadadi, M.; Moradi, A.; Yazdian, F.; Omidi, M. *International Journal of Biological Macromolecules* **2020**, *165*, DOI: 10.1016/j.ijbiomac.2020.09.166.

(26) Long, C.; Jiang, Z.; Shangguan, J.; Qing, T.; Zhang, P.; Feng, B. *Chemical Engineering Journal* **2021**, *406*, DOI: 10.1016/j.cej.2020.126848.

(27) Travlou, N. A.; Giannakoudakis, D. A.; Algarra, M.; Labella, A. M.; Rodríguez-Castellón, E.; Bandosz, T. J. *Carbon* **2018**, *135*, DOI: 10.1016/j.carbon.2018.04.018.

(28) Li, H.; Kang, Z.; Liu, Y.; Lee, S. T. *Journal of Materials Chemistry* **2012**, *22*, DOI: 10.1039/c2jm34690g.

(29) Qu, D.; Zheng, M.; Du, P.; Zhou, Y.; Zhang, L.; Li, D.; Tan, H.; Zhao, Z.; Xie, Z.; Sun, Z. *Nanoscale* **2013**, *5*, DOI: 10.1039/c3nr04402e.

(30) Lu, Y.; Wang, J.; Yuan, H.; Xiao, D. *Analytical Methods* **2014**, *6*, DOI: 10.1039/c4ay01052c.

(31) Hinterberger, V.; Damm, C.; Haines, P.; Guldi, D. M.; Peukert, W. *Nanoscale* **2019**, *11*, DOI: 10.1039/c9nr01029g.

(32) Kim, M.; Osone, S.; Kim, T.; Higashi, H.; Seto, T. *KONA Powder and Particle Journal* **2017**, *34*, DOI: 10.14356/kona.2017009.

(33) Reyes, D.; Camacho, M.; Camacho, M.; Mayorga, M.; Weathers, D.; Salamo, G.; Wang, Z.; Neogi, A. *Nanoscale Research Letters* **2016**, *11*, DOI: 10.1186/s11671-016-1638-8.

(34) Liu, C.; Zhao, Z.; Zhang, R.; Yang, L.; Wang, Z.; Yang, J.; Jiang, H.; Han, M.-Y.; Liu, B.; Zhang, Z. *Journal of Physical Chemistry C* **2015**, *119*, DOI: 10.1021/jp512918h.

(35) Han, L.; Ghosh, D.; Chen, W.; Pradhan, S.; Chang, X.; Chen, S. *Chemistry of Materials* **2009**, *21*, DOI: 10.1021/cm900709w.

(36) Ma, C.; Yin, C.; Fan, Y.; Yang, X.; Zhou, X. *Journal of Materials Science* **2019**, *54*, DOI: 10.1007/s10853-019-03585-7.

(37) Bourlinos, A. B.; Bakandritsos, A.; Kouloumpis, A.; Gournis, D.; Krysmann, M.; Giannelis, E. P.; Polakova, K.; Safarova, K.; Hola, K.; Zboril, R. *Journal of Materials Chemistry* **2012**, *22*, DOI: 10.1039/c2jm35592b.

(38) Zheng, M.; Ruan, S.; Liu, S.; Sun, T.; Qu, D.; Zhao, H.; Xie, Z.; Gao, H.; Jing, X.; Sun, Z. *ACS Nano* **2015**, *9*, DOI: 10.1021/acsnano.5b05575.

(39) Liu, X.; Jin, X.; Deng, H.; Sha, Z.; Zhou, X. *Journal of Nanoparticle Research* **2021**, *23*, DOI: 10.1007/s11051-021-05162-z.

(40) Vibhute, A.; Nille, O.; Kolekar, G.; Rohiwal, S.; Patil, S.; Lee, S.; Tiwari, A. P. *Journal of Fluorescence* **2022**, *32*, DOI: 10.1007/s10895-022-02977-4.

(41) Bourlinos, A. B.; Trivizas, G.; Karakassides, M. A.; Baikousi, M.; Kouloumpis, A.; Gournis, D.; Bakandritsos, A.; Hola, K.; Kozak, O.; Zboril, R.; Papagiannouli, I.; Aloukos, P.; Couris, S. *Carbon* **2015**, *83*, DOI: 10.1016/j.carbon.2014.11.032.

(42) Cai, Q. Y.; Li, J.; Ge, J.; Zhang, L.; Hu, Y. L.; Li, Z. H.; Qu, L. B. *Biosensors and Bioelectronics* **2015**, *72*, DOI: 10.1016/j.bios.2015.04.077.

(43) Chu, H. W.; Unnikrishnan, B.; Anand, A.; Lin, Y. W.; Huang, C. C. *Journal of Food and Drug Analysis* **2020**, *28*, DOI: 10.38212/2224-6614.1269.

(44) Kasprzyk, W.; Świergosz, T.; Bednarz, S.; Walas, K.; Bashmakova, N. V.; Bogdał, D. *Nanoscale* **2018**, *10*, DOI: 10.1039/c8nr03602k.

(45) Strauss, V.; Wang, H.; Delacroix, S.; Ledendecker, M.; Wessig, P. *Chemical Science* **2020**, *11*, DOI: 10.1039/d0sc01605e.

(46) Hou, Y.; Lu, Q.; Deng, J.; Li, H.; Zhang, Y. *Analytica Chimica Acta* **2015**, *866*, DOI: 10.1016/j.aca.2015.01.039.

(47) Nammahachak, N.; Aup-Ngoen, K. K.; Asanithi, P.; Horpratum, M.; Chuangchote, S.; Ratanaphan, S.; Surareungchai, W. *RSC Advances* **2022**, *12*, DOI: 10.1039/d2ra05989d.

(48) Pang, Z.; Fu, Y.; Yu, H.; Liu, S.; Yu, S.; Liu, Y.; Wu, Q.; Liu, Y.; Nie, G.; Xu, H.; Nie, S.; Yao, S. *Industrial Crops and Products* **2022**, *183*, DOI: https://doi.org/10.1016/j.indcrop.2022.114957.

(49) Zhang, H.; Wang, G.; Zhang, Z.; Lei, J. H.; Liu, T. M.; Xing, G.; Deng, C. X.; Tang, Z.; Qu, S. *Light: Science and Applications* **2022**, *11*, DOI: 10.1038/s41377-022-00798-5.

(50) Sousa, H. B.; Martins, C. S.; Prior, J. A. *Nanomaterials* **2021**, *11*, DOI: 10.3390/nano11030611.

(51) Liu, Q.; Zhang, N.; Shi, H.; Ji, W.; Guo, X.; Yuan, W.; Hu, Q. *New Journal of Chemistry* **2018**, *42*, DOI: 10.1039/c7nj05000c.

(52) Hagiwara, K.; Horikoshi, S.; Serpone, N. *Journal of Photochemistry and Photobiology A: Chemistry* **2021**, *415*, DOI: 10.1016/j.jphotochem.2021.113310.

(53) John, V. L.; Nair, Y.; Vinod, T. P. *Particle and Particle Systems Characterization* **2021**, *38*, DOI: 10.1002/ppsc.202100170.

(54) Jiang, K.; Sun, S.; Zhang, L.; Lu, Y.; Wu, A.; Cai, C.; Lin, H. *Angewandte Chemie* **2015**, *127*, DOI: 10.1002/ange.201501193.

(55) Wang, R.; Lu, K. Q.; Tang, Z. R.; Xu, Y. J. *Journal of Materials Chemistry A* **2017**, *5*, DOI: 10.1039/c6ta08660h.

(56) Kou, X.; Jiang, S.; Park, S. J.; Meng, L. Y. *Dalton Transactions* **2020**, *49*, DOI: 10.1039/d0dt01004a.

(57) Yang, S. T.; Cao, L.; Luo, P. G.; Lu, F.; Wang, X.; Wang, H.; Meziani, M. J.; Liu, Y.; Qi, G.; Sun, Y. P. *Journal of the American Chemical Society* **2009**, *131*, DOI: 10.1021/ja904843x.

(58) *3 Biotech* **2020**, *10*, DOI: 10.1007/s13205-020-02518-5.

(59) Gao, L.; Zhao, X.; Wang, J.; Wang, Y.; Yu, L.; Peng, H.; Zhu, J. *Optical Materials* **2018**, *75*, DOI: 10.1016/j.optmat.2017.11.044.

(60) Zhou, T.; Huang, Z.; Wan, F.; Sun, Y. *Materials Today Communications* **2020**, *23*, DOI: 10.1016/j.mtcomm.2020.100951.

(61) Mao, Q. X.; Wang, W. J.; Hai, X.; Shu, Y.; Chen, X. W.; Wang, J. H. *Journal of Materials Chemistry B* **2015**, *3*, DOI: 10.1039/c5tb00963d.

(62) Garcia, Y. S.; Barros, M. R.; Ventura, G. T.; de Queiroz, R. M.; Todeschini, A. R.; Neves, J. L. *Journal of Molecular Liquids* **2019**, *292*, DOI: 10.1016/j.molliq.2019.111460.

(63) Abbasi, S.; Paul, A.; Shao, W.; Prakash, S. *Journal of Drug Delivery* **2012**, *2012*, DOI: 10.1155/2012/686108.

(64) Jian, H. J.; Wu, R. S.; Lin, T. Y.; Li, Y. J.; Lin, H. J.; Harroun, S. G.; Lai, J. Y.; Huang, C. C. *ACS Nano* **2017**, *11*, DOI: 10.1021/acsnano.7b01023.

(65) Hashemkhani, M.; Loizidou, M.; Macrobert, A. J.; Acar, H. Y. *Inorganic Chemistry* **2022**, *61*, DOI: 10.1021/acs.inorgchem.1c03298.

(66) Mondal, T. K.; Mondal, S.; Ghorai, U. K.; Saha, S. K. *Journal of Colloid and Interface Science* **2019**, *553*, 177–185.

(67) Díez-Pascual, A. M. *Materials* **2022**, *15*, DOI: 10.3390/ma15093251.

(68) Srivastava, I.; Khamo, J. S.; Pandit, S.; Fathi, P.; Huang, X.; Cao, A.; Haasch, R. T.; Nie, S.; Zhang, K.; Pan, D. *Advanced Functional Materials* **2019**, *29*, DOI: 10.1002/adfm.201902466.

(69) Pastorizo-Santos, I.; Liz-Marzán, L. M. *Advanced Functional Materials* **2009**, *19*, DOI: 10.1002/adfm.200801566.

(70) Christ, H. A.; Bourgat, Y.; Menzel, H. *Polymers* **2021**, *13*, DOI: 10.3390/polym13162702.

(71) Panalytical, M. *Dynamic Light Scattering: An Introduction in 30 Minutes*; Malvern Panalytical, 2023.

(72) Panalytical, M. *ZetaPotential-Introduction-in-30min-Malvern*; 2015.

(73) Max, J. J.; Chapados, C. *Journal of Physical Chemistry A* **2004**, *108*, DOI: 10.1021/jp036401t.

(74) Zhu, H.; Wang, X.; Li, Y.; Wang, Z.; Yang, F.; Yang, X. *Chemical Communications* **2009**, DOI: 10.1039/b907612c.

(75) Lawson-Wood, K.; Upstone, S.; Evans, K. *Determination of Relative Fluorescence Quantum Yields using the FL 6500 Fluorescence Spectrometer*; 2018.

(76) Bashkatov, A. N.; Genina, E. A. *Water refractive index in dependence on temperature and wavelength: a simple approximation*; 2003.

(77) Gyulai, G.; Ouanzi, F.; Bertóti, I.; Mohai, M.; Kolonits, T.; Horváti, K.; Bősze, S. *Journal of Colloid and Interface Science* **2019**, *549*, DOI: 10.1016/j.jcis.2019.04.058.

Summary

Name: Bryan Steven Chiguano Tapia

Neptun: GYSLIX

ELTE Faculty of Science: MSc Materials Science

Title of diploma work: Surface Modification of Fluorescent Carbon Quantum Dots.

Carbon quantum dots are the newest nanomaterials that offer versatile applications. Their distinctive characteristics, such as tunable photoluminescence, biocompatibility, and low toxicity, make them highly useful. To optimize their stability, solubility, and functionality, surface modifications are crucial during and after synthesis. To exploit CQDs' maximum potential, effective surface modification is essential. In this study, CQDs were synthesized and subsequently modified through chemical and physical processes. HOBt and EDC were utilized as binding agents, while EDA, ETA, and PEI were used as surface modifiers. The chemical modification involved EDA, ETA, and PEI, while physical modification solely relied on PEI. UV-Vis, fluorescence, and ATR-IR spectroscopy were employed for the characterization of both raw and modified CQDs. Additionally, DLS experiments provided insights into particle size through hydrodynamic diameter analysis, and electrophoretic mobility tests enabled the determination of particle surface charge through zeta potential values. Characterization experiments provided a valuable understanding of the properties of CQDs. DLS experiments confirmed their small size and zeta potential analysis supported their high stability and surface charge. ATR-IR spectroscopy identified the chemical composition, while fluorescence experiments showed consistent excitation and emission peaks with varying intensities. The chemically modified samples showed lower quantum yield values than the physically modified ones, opening up the potential for enhancing it through fine-tuning chemical modification parameters in future studies. Specifically, further investigation can focus on their effectiveness in peptide modifications, affinity towards bacterial membranes, and interactions with living membranes in terms of polarity. Advancing research in these areas will enhance our understanding of the potential applications of modified CQDs, leading to new opportunities for their use and contributing to scientific advancements in multiple disciplines.